Published in final edited form as:
Magn Reson Med. 2014 April ; 71(4): 1358–1367. doi:10.1002/mrm.24814.

MRSI of the Medial Temporal Lobe at 7T in Explosive Blast Mild Traumatic Brain Injury

HP Hetherington[1,3], **H Hamid**[4,6], **J Kulas**[5,7], **G Ling**[8], **F Bandak**[8,9], **NC de Lanerolle**[3], and **JW Pan**[2,3]

[1]Department of Radiology, University of Pittsburgh

[2]Department of Neurology, University of Pittsburgh

[3]Department of Neurosurgery, Yale University School of Medicine

[4]Department of Neurology, Yale University School of Medicine

[5]Department of Psychiatry, Yale University School of Medicine

[6]Department of Neurology, West Haven Veterans Administration Medical Center

[7]Department of Psychiatry, West Haven Veterans Administration Medical Center

[8]Department of Neurology, F. Edward Hébert School of Medicine, Uniformed Services University of the Health Sciences, Bethesda, MD

[9]Integrated Services Group, Inc., Potomac, MD

Abstract

Purpose—Up to 19% of veterans returning from the wars in Iraq and Afghanistan have a history of mild traumatic brain injury (mTBI) with 70% associated with blast exposure. Tragically, 20–50% of this group reports persistent symptoms, including memory loss. Unfortunately, routine clinical imaging is typically normal, making diagnosis and clinical management difficult. The goal of this work was to develop methods to acquire hippocampal MRSI at 7T and evaluate their sensitivity to detect injury in veterans with mTBI.

Methods—At 7T, hippocampal MRSI measurements are limited by: 1) poor B_0 homogeneity; 2) insufficient B_1^+ strength and homogeneity; and 3) chemical shift dispersion artifacts. To overcome these limitations we: 1) used 3rd degree B_0 shimming; 2) an inductively decoupled transceiver array with RF shimming and 3) a volume localized single slice sequence using RF shimming based outer volume suppression.

Results—In 20 controls and 25 veterans with mTBI due to blast exposure with memory impairment, hippocampal NAA/Cho ($P<0.001$) and NAA/Cr ($P<0.001$) were decreased in comparison to control subjects.

Contact Information, Hoby Hetherington, Professor, Department of Radiology, University of Pittsburgh, B820 PUH, 200 Lothrop St., Pittsburgh, PA 15213, hetheringtonh@upmc.edu, 914-433-5783.

Conclusion—With the appropriate methods robust spectroscopic imaging of the hippocampus can be carried out at 7T. MRSI at 7T can detect hippocampal injury in veterans with mild traumatic brain injury.

Keywords

mild traumatic brain injury(mTBI); MRSI; hippocampus; 7T

With the wars in Afghanistan and Iraq, mild traumatic brain injury, mTBI, from explosive blast exposure is reaching dramatic proportions. It is estimated that approximately 23% of veterans report being physically moved or knocked over by blast exposure (1). It is also estimated that 1 in 5 returning veteran warfighters have a history of TBI (2) with 70% being associated with blast exposure (3). Although controversial, some estimates report 20 – 50% of that group report some form of dysfunction one year post injury (4–7). The clinical assessment of this type of injury is difficult on several levels. First, accurate and independent details as to the severity of the blast are not generally available. Second, while the symptoms include impaired memory and concentration, irritability, sleep disorders and PTSD, cognitive testing to quantify these problems can be inconclusive and complicated by factors that can influence the validity of that report including psychiatric and motivational concerns. Although the presence of poor effort and symptom magnification on objective cognitive and psychological assessment can be identified through the use of symptom validity measures, once it is identified the validity of the entire evaluation is called into question, even where legitimate injury is suspected (8–10). Thus, a finding of symptom magnification leaves few options for objective assessment (11, 12). With effort failure rates of 17 to 58% in veterans with mTBI (13, 14), methods able to objectively identify the presence of injury and anatomically link it with specific cognitive domains could significantly impact treatment prioritization and clinical management.

Despite the obvious significance and large numbers of returning veterans with blast mTBI, there have been relatively few reports of neuroimaging studies demonstrating significant injury. While conventional structural imaging studies have been generally negative, PET and diffusion studies have reported significant changes in veterans with mTBI related to blast exposure. Mac Donald and colleagues reported an increased number of DTI abnormalities in 18 of 63 veterans with TBI related to blast with additional associated head impact events (15). Studies with smaller numbers of patients have reported changes in DTI with blast related TBI and depression (16) and hypometabolism in the cerebellum (17). However, a recent study failed to find differences in fractional anisotropy in those with mTBI (18).

In conventional non-blast TBI, MRS measurements of decreased N-acetyl aspartate, NAA, levels have been reported in MRI-normal brain regions (19) and have been used to predict long term cognitive outcome in children (20) and adults (21). In athletes who have experienced a sport-related concussive head injury (with or without loss of consciousness) reductions in NAA have been reported in frontal white matter which persisted beyond the resolution of clinical symptoms, and whose recovery was significantly slowed by exposure to a second concussive injury (22). Similarly, Henry and colleagues recently reported chronic changes in football players that persisted 6 months after concussion injury (23).

Based on these findings, we initiated a study evaluating alterations in the ratios of NAA to Choline (NAA/Cho) and NAA to Creatine (NAA/Cr) in veterans with a history of mTBI associated with blast exposure who reported ongoing memory impairment. Given the prevalence of memory symptomatology in this group, we targeted the medial temporal lobes for this spectroscopic imaging study at 7T.

Although 7T offers significant advantages in terms of increased signal to noise ratio (SNR) (24), spectroscopic imaging measurements of the human hippocampus at 7T are challenging. Due to the proximity of the medial temporal lobe to the frontal sinuses and ear canals, spectral quality is degraded by susceptibility effects which increase linearly with field strength. Although good B_1^+ homogeneity can be achieved with transverse electromagnetic, TEM, volume coils for superior brain locations (25), high frequency RF effects dramatically degrade homogeneity in the temporal lobes resulting in a two-fold variation in B_1^+, decreasing SNR by the use of non-optimal pulse angles. Similarly, the decreased available B_1^+ strength at 7T versus 3T results in substantial chemical shift dispersion artifacts for MRSI sequences using large bandwidth in-plane slice selective pulses. To overcome the limitations in B_0 homogeneity we used 3rd degree B_0 shimming with an ROI targeting the medial temporal lobe (26, 27). To obtain good B_1^+ homogeneity we used an 8 element inductively decoupled transceiver array with RF shimming (28). To minimize chemical shift dispersion errors, we used a volume localized a single slice moderate TE sequence with RF shimming based outer volume suppression to provide in-plane localization (29). We used these methods to acquire data from 20 control subjects and 25 veterans with self-reported memory impairment and a history of explosive blast mTBI. The MRSI data revealed highly significant declines in NAA/Cho ($P<0.001$) and NAA/Cr ($P<0.001$) from the most anterior regions of the hippocampi in comparison to control subjects. This data represents one of the first studies to identify significant MR-detected abnormalities in veteran warfighters with blast mTBI associated with a specific anatomical domain and its correlated deficit.

METHODS

RF coil and B_0 Shimming

All data were acquired with an Agilent Direct Drive console and a head only (68cm ID) actively shielded 7T magnet. An 8 coil inductively decoupled transceiver array was used for all studies. The array was built with a split design consisting of two sections, a posterior section with 5 coils and an anterior section with 3 coils (30). The posterior section had a width in the left right direction of 19.5cm. Two different anterior sections were used so as to accommodate different head sizes in the anterior-posterior (AP) direction. When the two sections were combined, the array measured 23 and 25cm respectively in the AP direction. The individual coils in the array were rectangular in shape and measured 9cm × 9cm (length × width in circumferential direction) for the posterior array and the 23 cm anterior array, while the 25cm anterior array used 9cm×10cm coils. The array was positioned so as to place the medial temporal lobes within the center of the array subject to constraints of individual variations in anatomy.

The gradient system (Agilent) included a full set of 2nd and 3rd degree shims, with each shim driven by two 10A shim power supplies (Resonance Research Inc.). A non-iterative

multi-slice B_0 mapping method was used to acquire B_0 maps, calculate necessary shim currents and set all currents (27, 31). The B_0 maps were generated using 5 evolution periods, corresponding to additional delays of 0 (for reference), 1, 2, 4 and 8ms. The B_0 maps were acquired using 11 slices with a thickness of 2mm and a gap of 2mm, such that the 10mm SI slice thickness was spanned by three B_0 map slices. The ROI for the shim optimization was determined using scout images. With each B_0 map acquisition, the measured and predicted (i.e., after shim correction) standard deviation of the B_0 field over the ROI, σB_0^{Global} was calculated. For verification of the predicted map, a second B_0 map was acquired after shimming. The measured and predicted inhomogeneity, over the selected ROI, typically varied by less than 1Hz for a single iteration of shimming. To provide an estimate of the line-width, maps of local inhomogeneity, σB_0^{Local} were calculated from the standard deviation over a 3×3×3 region of B_0 pixels (26). Assuming a gaussian distribution, the line-width, full width at half maximum - FWHM, is given by $2.35\,\sigma B_0^{Local}$. Performance data for B_0 shimming was compiled using the initial 15 subjects in each of the mTBI and control groups.

Pulse Sequence and RF Shimming

Spectroscopic imaging data were acquired using a moderate (40ms) TE sequence to minimize spectral overlap of NAA, creatine and choline with J-modulating compounds. Localization using the 8 element elliptical transceiver included a combination of gradient based slice-selective excitation and RF shimming based outer volume suppression (28, 29). As previously described, we used two RF distributions (“homogeneous” and “ring”) determined in each volunteer by B_1 mapping and optimization.

The maximum 10g average for SAR was calculated using Remcom XF7.1.0.5 (REMCON Corporation, College Station, PA) Finite Difference Time Domain (FDTD) electromagnetic wave analysis was used for B_1^+, electric field (E) and SAR calculations. All coils within the array were numerically matched to better than -20dB at the same frequency (±0.5MHz). The inductive decoupling between each surface coil pair was modeled using a Thevenin lumped circuit equivalent of a transformer. The values of the individual inductors were iteratively adjusted to achieve the target decoupling of typically better than -15dB (similar to that seen in vivo better than -16dB isolation (28)). Simulations were performed using a head model with tissue parameters (at 7T) calculated by the Cole-Cole method (25). The simulation was calculated using a variable grid size ranging from less than 1mm (enabling small structural details in the transceiver and head to be accurately represented) to a base cell size of 30mm in air/free space. The amplitude and phase values for the homogeneous and ring distributions for the individual coils in the array were determined using the same RF shimming procedures as described for the in vivo studies, with the exception that the maximum power for a coil in the ring distribution was not constrained by a maximum value. The slice was angulated by 20° matching that used in the in vivo studies. These values were then used to calculate the 10g averages for SAR for simultaneous transmission for the two different RF distributions.

MRSI Acquisition, Processing and Analysis

The target slice (10mm thickness, 300Hz/mm gradient slice selection strength) was angulated along the temporal pole, approximately 20 degree, at the level of the hippocampus. Rectangular phase encoding (24×24) was performed over a FOV of $192\times192mm^2$. The TR was 1.5s resulting in an acquisition time of 14.4min. To provide phase and amplitude scaling for optimal SNR for the reconstruction of the metabolite SI data, an unsuppressed water SI was acquired using the same sequence but without water suppression and TR=0.5s as previously described (28).The metabolite data in each pixel was then divided by the integrated area of the unsuppressed water signal from the corresponding pixels in the unsuppressed water SI. Although this corrects for the spatial dependence of the reception efficiency due to array reception, it does not correct for differences in T1, T2 or water content. The data were processed with 4Hz of Gaussian broadening (FWHM), in the spectral domain and a hanning filter in the spatial domain.

Spectroscopic data were processed using semi-automatic anatomically guided reconstructions (32) so as to account for variations in metabolite ratios along the length of the hippocampal formation. The hippocampi were manually outlined on T1 weighted images (Fig. 1A red and green lines) and a midline is automatically calculated (blue). The aqueduct is then identified and six voxels (three anterior, one centered at the aqueduct and two posterior to the aqueduct) are reconstructed from the MRSI data at 9mm increments along the midline. The voxels were then labeled from 1 to 6, with voxel 1 being the most posterior pixel. Spectra were fit in the time domain using Gaussian line-shapes and the ratios of NAA/Cho and NAA/Cr were calculated using resonance areas. No attempt was made to resolve NAA and N-acetyl glutamate. All images and spectroscopic images are presented using the convention that the left portion of the image corresponds to the subject's right side.

Hippocampal Volume Measurements

The volume of the right and left hippocampus were determined by manual tracing (33) on 1.5mm isotropic T1 weighted images. Due to known differences between brain size in men and women and the high fraction of men in the mTBI group; only data from men in mTBI and control groups were used for comparison.

Statistical Evaluation

The data was grouped according to location (1–6), side (right or left) and patient versus control subject. A two tailed T-test was carried out to evaluate for potential statistical differences between equivalent loci. The data was then divided into two families of data, NAA/Cr and NAA/Cho ratios. To correct for potential type I errors (i.e. false discovery of significant differences) and retain statistical power to avoid type II errors (failure to detect true significant differences) for each family of measures, a Benjamini-Hochberg (34) test was used with the false discovery rate set to be 5% or less.

Subject Enrollment

20 control subjects (32±12 years, 12 men) and 25 veteran warfighters (34+9 years, 24 men) with blast related mTBI were studied with prior approval of the Yale Committee on Human Investigations and the West Haven Veterans Administration Institutional review Board.

mTBI was defined as a traumatically induced disruption of brain function using the criteria of Center for Disease Control (35). The number of blast exposures in veterans ranged from 1 to more than 10, with all reported exposures being more than 1 year prior to the MRSI study. Due to the commonality of symptoms between PTSD and mTBI (36), the veterans were evaluated by a board certified psychiatrist for PTSD, depression, anxiety and substance dependence using the Diagnostic and Statistical manual of Mental Disorders Fourth Edition criteria, PTSD Check List (PCL-M), Beck Depression Inventory II and Beck Anxiety Inventory. Cognitive assessments included the evaluation of verbal and visual memory (California Verbal Learning Test 2nd Edition, Rey-Osterrieth Complex Figure Test) and effort testing (Test of Memory Malingering and Green's Word Memory Test). Potential control subjects reporting a history of psychiatric or neurologic illness were excluded from the study.

RESULTS

3rd Degree B_0 Shimming

Fig. 2 displays the tailored ROIs (Fig. 2A) used for shimming the medial temporal lobe. The resulting B_0 and σB_0^{Local} maps attained using only 2nd degree shims (as available on most 7T systems) and 3rd degree shims are displayed in Figs. 2B and 2C. The tailored ROI uses a 100mm circular region with an elliptical cutout to focus the shimming on the medial temporal lobe. The ROI is designed to minimize the role of susceptibility effects from the ear canals (lateral to the ROI) and frontal sinus (anterior) to the ROI from degrading the homogeneity over the medial temporal lobe. As a group the residual B_0 inhomogeneity, σB_0^{Global}, was reduced by 39% from 17.6±3.6 to 11.1±2.4Hz when adding 3rd degree shims to 1st&2nd degree shims (Fig. 2B). Consistent with the large improvement, a large third order residual having C3 symmetry is seen in the B_0 map when using only 1st & 2nd degree shims. The predicted effect of improved shimming on spectral quality can be seen in the σB_0^{Local} maps (Fig. 2C). In this case (Fig. 2C) σB_0^{Local} in the anterior regions of the hippocampi approach 15–20Hz when only 2nd degree shims are used. When 3rd degree shimming is added, σB_0^{Local} decreases to ~10Hz or less. Consistent with the σB_0^{Local} maps, the largest improvement with 3rd degree shimming is achieved in the most anterior loci (Figs. 2D and 2E). In this case when using 2nd degree shimming, the most anterior rows of the hippocampal formation (green ROI – spectra far right Fig. 2D) show substantial overlap between Cr and Cho with substantially broader lines. In comparison, with 3rd degree shimming (Fig. 2E) B_0 homogeneity is maintained and creatine and choline are resolved to near baseline. There were no significant differences in σB_0^{Local} between patients and control subjects.

Effect of using a tailored ROI

To evaluate the improvement in homogeneity afforded by use of the tailored ROI when using 3rd degree shims, we calculated σB_0^{Global} and σB_0^{Local} using with the tailored ROI (Fig. 2A) and a whole slice ROI (an ROI including all of the brain within the slice). When using the tailored ROI to optimize the shims as opposed to the whole slice ROI, over the group of

30 subjects σB_0^{Global} decreased by 21% from 13.9±2.9 to 11.1±2.4. On an individual by individual basis the improvement in σB_0^{Global} ranged from 9 to 32%. To evaluate the improvement in σB_0^{Local} for the hippocampal loci when using the tailored ROI, we calculated σB_0^{Local} over the 12 pixels spanning the hippocampal formations using the two ROIs. The group data is displayed in Table 1. Reductions in σB_0^{Local} ranged from 8 to 23%. Notably the mean reduction in line width, full width at half height, provided by using the tailored ROI is 7.5Hz (2.35 σB_0^{Local}) in voxel 6, the most anterior location.

B_1^+ Distributions and RF Shimming

Due to the angulation used for the hippocampal slice and the relatively short length of the coil (9cm), the anterior portion of the selected slice was typically located immediately below the inferior edge of coils 4–6 of the array. In contrast, the posterior portion of the slice was located more towards the middle of the array beneath coils 1, 2 and 8. Due to the requirement that the head be placed deeply into the coil with the nose within the active elements, the anterior coils were typically farther from the brain than the posterior or lateral coils. For equivalent drive voltages, the achieved B_1^+ varies significantly with the posterior coils having the strongest B_1^+ within the selected slice, followed by the lateral coils, with the anterior coils having the weakest B_1^+ (Fig. 3A). As expected, use of equal drives results in B_1^+ poor homogeneity, with a standard deviation of 22% over the ROI stemming from insufficient B_1^+ in the anterior and excess B_1^+ in the posterior (Fig. 3B). A B_1^+ map following RF shimming for the homogeneous distribution is displayed in Fig. 3C, which achieves a standard deviation of 11%. To assess the variations on a group basis we evaluated the power required for each distribution in 10 studies with 5 studies in each of the two coil configurations (23 and 25cm AP). Due to a variety of factors including: distance to the brain (anterior coils are further away), positioning of the slice relative to the longitudinal axis of the coil (the anterior portion of the selected slice is closer to the inferior edge of the coil) the required power for each coil varied significantly, necessitating RF shimming (Table 2). Despite this variability, the standard deviation of the B_1^+ over the ROI (virtually all of the brain within the slice) was 12.7±1.9%. The 23cm coil achieved a mean B_1^+ of 940Hz (5 subjects) at 2.21kW, while the 25cm coil (5 subjects) achieved a mean B_1^+ of 888Hz at 2.65kW.

For the ring distribution, due to its highly constructive nature at the periphery of the head (29), the maximum output of any individual channel was constrained to 35% of its maximum output voltage or ~140W, to limit the local SAR. Similarly, the lateral coils also showed an increased required power. Despite these factors, there is sufficient B_1^+ in the peripheral regions, when combined with adiabatic inversion pulses to provide sufficient suppression of extracerebral lipids from the target ROI (Fig. 3C). Notably, since the ring distribution uses only RF shimming to generate spatial localization (i.e. no gradients are applied) chemical shift dispersion artifacts are eliminated.

RF Power Deposition

Based on the FDTD simulations, the 10g averages for the maximum SAR for 1W of input over the entire head were 0.90 and 2.35W/kg for the homogeneous and ring distributions

respectively. To estimate the maximum SAR for the pulse sequence we summed the contributions of the two distributions weighted by their duration, RF shapes and output levels used for the 10 subjects (Table 2). The mean deposited total power was 4.73±0.61W and the maximum SAR for a 10g average was 6.15±0.69W/kg. Notably the anatomical locations of the maximum SAR vary for the two distributions and do not coincide spatially due to the different phase relationships used. In general the maximum SAR for the homogenous distribution is located at the longitudinal edge of the RF coil where the E fields are generally constructive, while the ring distribution provides greater SAR from more central locations within the coil where the E-fields are more constructive. For safety purposes, the calculation of SAR for the pulse sequence assumes that the loci of maximum SAR are the same for the two sequences. Although the ring distribution shows a much higher maximum SAR for equivalent input as the homogeneous distribution, the much higher efficiency of the ring distribution at the peripheral locations (29) results in lower required power overcoming the increase in SAR.

Anatomical Variations in Metabolite Ratios in Controls

Displayed in Table 3 are data from control and patient subjects using the semi-automated reconstructions. Consistent with the spectral data shown in Figs. 1 and 2, the ratio of NAA/Cho in control subjects declines markedly along the length of the hippocampal formation, ranging from 1.77+0.15 (locus #1 - posterior right) to 0.99±0.16 (locus 6 - anterior left). NAA/Cr ratios in controls showed a similar dependence, 1.47±0.15 to 1.17+0.16 (loci 1 left and 5 right respectively). No significant difference was seen in the NAA/Cr or NAA/Cho ratios between the left or right hemisphere for equivalent locations along the hippocampal formations in controls.

Comparison of Patient and Control data

Displayed in Fig. 4 are data from a veteran with multiple blast exposures who does not suffer from PTSD. A large decrease, exceeding 2SDs, in NAA/Cho in comparison to the control group is seen along both hippocampal formations (Fig. 4B). The differences are most pronounced from the most anterior loci (#6) (Fig. 4C). Using $p<0.05$ for individual T-tests, as a group the veterans with mTBI displayed significant reductions ($p<0.05$) in NAA/Cho from loci 2–6 from right hippocampus, and loci 5 and 6 on the left in comparison to the control group. After controlling for a false discovery rate using the Benjamini-Hochberg test, all of the loci identified with $p<0.05$ were found to be significantly different from their corresponding control location. Using T-tests, NAA/Cr in the mTBI group was significantly lower than controls in loci 4–6 from the right hippocampus. No loci in the left hippocampus achieved $p<0.05$ on individual T-tests for NAA/Cr. After controlling for a false discovery rate using the Benjamini-Hochberg test, loci 4 and 6 were found to be significantly different from their corresponding control location. The volume of the right hippocampus of the mTBI subjects were significantly smaller ($p=0.001$) 3.39±0.36 than controls 4.01±0.36. The left hippocampus for mTBI subjects 3.73±0.35 was not significantly different ($p=0.51$) from control subjects 3.83±0.35.

To corroborate the self-reported memory impairment, cognitive tests assessing memory performance were carried out. As a group, the veterans displayed reduced performance for

verbal and visual memory related tasks including cued recall, short term recall and long term recall. The reductions in Z scores ranged from Z=−0.33 to Z=−0.67. To evaluate the potential role that psychiatric co-morbidities might be solely responsible for the differences seen in NAA/Cho and NAA/Cr in this group in comparison to controls, we grouped the data according to whether or not the patients also had a diagnosis of PTSD (16/25), depression (15/25), anxiety (10/25) or are ethanol dependent (5/21). For other drugs of abuse (cocaine, cannabis and opioids) at most a single subject reported dependence in each category, thus no statistical evaluation was made. Those loci identified from the previous analysis as significantly different after correction for false discovery rate of 0.05, were then compared using a two tailed T-test. No statistically significant differences were seen in the group data when comparing mTBI subjects with and without a specific comorbidity (e.g. mTBI without PTSD versus mTBI with PTSD) from any locus. The fractional differences in mean values between the groups ranged from -15% (the non-depressed veterans had a lower NAA/Cho ratio in locus 6 right) to +5% (the ethanol dependent veterans had a lower NAA/Cho ratio in locus 5 right). Thus as a whole, presence or absence of a specific co-morbidity did not significantly alter the mean value reported from the group.

DISCUSSION

B_0 Shimming

The use of the localized ROI significantly enhances homogeneity over the target ROI by allowing the optimization routines to “ignore” the very high degree inhomogeneities arising from the ear canals and frontal sinus. Over the restricted ROI, addition of 3rd degree shim corrections to 1st & 2nd degree corrections resulted in a 37% improvement in homogeneity. This independent data is consistent with our previous work (26) where the achieved homogeneity improved by 37% when including third degree shims reaching a similar value of σB_0^{Global} of 10.5Hz (11.1Hz in this group). This is most strongly seen from the anterior loci of the hippocampal formations. With only 2nd degree shims, there is substantial overlap between Cho and Cr, along with broad baseline distortions. In contrast, addition of 3rd degree shims enables resolution of Cho and Cr to baseline and minimizes distortions in the baseline. In the data from the subject displayed in Fig.2, σB_0^{Global} for 3rd degree shimming was 11.7Hz, slightly larger than the average for the group, 11.1Hz. In this population of veterans, statistically significant changes are predominantly seen in the most anterior loci, with the largest changes seen in locus 6. Thus, attaining sufficient B_0 homogeneity and spectral quality in the anterior hippocampal formation is critical for detection of the injury.

To determine the potential improvement with increasing shim degree we calculated the residual inhomogeneity using up to 14th degree shims (Fig. 5). As can be seen σB_0^{Global} reaches an asymptote at 7th degree, with only minimal improvement above that level. With 3rd degree shims, the dominant inhomogeneities over the tailored ROI arise from the ear canals and frontal sinus. Addition of 4th degree shims (26) should significantly improve the B_0 homogeneity in the regions immediately above the ear canals and the anterior regions of the hippocampal formations. The calculated homogeneity above 7th degree is 5.17Hz, with the inhomogeneity dominated by susceptibility effects from vessels and gray/white matter differences.

B_1 Shimming

For the strongly angulated slice, use of equivalent drive amplitudes to all coils in the array results in marked inhomogeneity (22%) over the target ROI. The need for RF shimming and significantly different drive voltages is due to the greater distance of the head to the anterior coils and the positioning of the anterior portion of the slice generally closer to the inferior edge of the coil. For the relatively short array used, the B_1^+ generated at the longitudinal edges of the array is generally less than that in the central region of the array. Despite these issues, after B_1^+ shimming the SD over the selected ROI in this subject was reduced from 22% to 11%. As a group, the SD of the B_1^+ for the homogeneous distribution was 12.7%. Notably, the same RF phases were used for both the RF amplitude shimmed and non-shimmed distributions. For the ring distribution a similar effect was seen, with significantly higher drive voltages used for the anterior coils. Despite these challenges, good suppression of the extracerebral lipid signals arising from the temporalis muscle and skin was obtained over the target ROI for the MRSI study.

Patient Data

This data represents one of the first studies to identify consistent significant changes reflective of injury in blast related mTBI. The changes seen, reductions in NAA/Cho and NAA/Cr in comparison to controls are consistent with the potential presence of neuronal and axonal injury. The smaller volume of the right hippocampus (as opposed to left) in comparison to controls is consistent with the reduction in NAA/Cr seen in the right hippocampus, and the greater spatial extent of changes in NAA/Cho also seen from the right hippocampus. The smaller hippocampus, primarily a gray matter structure, may result in increases in CSF content and the fraction of white matter/gray matter content in the volumes measured. An increase in CSF content combined with a partial volume shift due to gradient based slice selection can potentially cause an artifact in metabolite ratios, since the measured volumes for NAA, Cr and Cho no longer come from the same locations. However, the use of ring based outer volume suppression and a 300Hz/mm slice selection gradient limits the shift between NAA and Cr and NAA and Cho volumes to 1.0 and 1.2mm (10 and 12% respectively) in the slice direction. An increase in the fractional content of white matter can also modify metabolite ratios independent of any pathology. However increasing fractional white matter content in the absence of any other change will tend to increase NAA/Cr ratios due to the naturally higher ratios of NAA/Cr in white matter as opposed to gray matter (37).

The anatomical site of these changes, the hippocampal formation, is consistent with the self-reported memory impairment, the poorer cognitive performance scores seen from the group, and the role of the hippocampus and temporal lobe in tasks related to memory. All mTBI subjects were evaluated at least one year prior to study, with the duration between the study and the last blast related event being 1–10 years. Since the status of the subjects before and immediately after the mTBI is not known, the extent of recovery and/or progression of injury cannot be determined in this study. Regardless of the temporal characteristics, reduced NAA/Cr, NAA/Cho, hippocampal volumes and cognitive impairment is present more than one year from the date of the initial injury.

The exact mechanism by which blast mTBI results in persistent injury and cognitive deficits is unknown; however the involvement of the hippocampus has been reported in several animal models of blast injury including the rat (38–40), pig (41) and primate (42). Notably, the anterior hippocampal locations include a portion of the amygdala, a site involved in emotional processing. It is possible that damage to the hippocampus may also play a role with the high comorbidity of PTSD 44% (see (36) for review). Alternatively, some investigators have proposed that the symptoms seen in blast related mTBI may be largely attributable to PTSD (43). However, in this small group, there were no significant differences between mTBI subjects with (or without a diagnosis of PTSD, depression, anxiety or ethanol dependence.

In this group of veterans 10 of the 25 displayed NAA/Cho declines more than two standard deviations from control values for locus 6 right (locus of greatest decline). Of the 21 veterans who completed effort testing, 7 failed their effort tests. Amongst the small group that failed effort testing, all had NAA/Cho ratios from locus 6 right below the mean for controls with a mean value of 0.80±0.16, more than 1.5SDs from control values. Additionally, three veterans who failed effort testing, had NAA/Cho ratios (0.62–0.66) in locus 6 right more than 2 SDs from control. For veterans who fail effort testing, deficits in performance on other neurocognitive assessment measures and claims of impairment are open to question, challenge and dismissal. Given the multitude of psychological processes that can lead to poor performance on these measures, it is uncertain whether or not the poor performance on symptom validity assessment is directly attributable to the processes giving rise to the reduced NAA/Cho. Regardless, the presence of a large deficit in NAA/Cho is consistent with neuronal injury in this brain region. Thus, an objective imaging measure of dysfunction has a clear role in the management of these patients as a means to identify the presence of injury in cases of self-reported memory impairment. Finally, the extent to which measurements of NAA/Cho are quantitatively predictive of the degree of memory impairment in blast mTBI will require additional studies.

Although the dramatic decreases in NAA/Cho from the most severely affected patients are detectable from conventional grid based reconstructions there is a very strong anterior-posterior dependence in NAA/Cho and a weaker, although still significant dependence for NAA/Cr. Thus, the use of the anatomically driven reconstructions enables a more accurate comparison of patient and control data by correcting for anatomical location. The origin of the positional dependence of NA/Cho ratios along the hippocampal formation may be due to metabolic/cellular differences from different hippocampal subfields such as CA1–4, the dentate gyrus and subiculum along its length. The contributions of the amygdala to the anterior loci of the hippocampal formation may also be a factor.

Finally, as described, the most profound decreases in NAA/Cho and NAA/Cr in the mTBI group were seen in the most anterior loci of the hippocampal formations. This highlights the importance of higher degree shimming, as the largest absolute improvements in σB_0^{Local} (in Hz) are seen from the same loci. As shown in Fig. 2, the improvement in σB_0^{Local} translates into an improvement in line-width and spectral quality. This is consistent with our previous work demonstrating a strong linear relationship between σB_0^{Local} and line-width in the

hippocampus (26). Thus in this study, access to higher degree shimming at 7T was a critical component leading to improved data quality and likely the overall success of the study.

Acknowledgments

This work was supported by grants from the NIH R01EB009871, R01EB011639, R01NS081772 and DARPA/SPAWAR N66001-08-C-2005.

REFERENCES

1. Tanielian, T. Assessing Combat Exposure and Post-Traumatic Stress Disorder in Troops and Estimating the Costs to Society Implications from the RAND Invisible Wounds of War Study. In: SoDAaMA. , editor. House Veterans' Affairs Committee. RAND Corporation; 2009.
2. Tanelian, T.; Jaycox, L. Invisible Wounds of War Psychological and Cognitive Injuries, Their Consequences, and Services to Assist Recovery. Santa Monica: Rand Corporation; 2008.
3. Warden D. Military TBI during the Iraq and Afghanistan wars. J Head Trauma Rehabil. 2006; 21(5):398–402. [PubMed: 16983225]
4. Vasterling JJ, Verfaellie M, Sullivan KD. Mild traumatic brain injury and posttraumatic stress disorder in returning veterans: perspectives from cognitive neuroscience. Clin Psychol Rev. 2009; 29(8):674–684. [PubMed: 19744760]
5. Bass CR, Panzer MB, Rafaels KA, Wood G, Shridharani J, Capehart B. Brain injuries from blast. Ann Biomed Eng. 2012; 40(1):185–202. [PubMed: 22012085]
6. Sayer NA. Traumatic brain injury and its neuropsychiatric sequelae in war veterans. Annu Rev Med. 2012; 63:405–419. [PubMed: 22248327]
7. Rosenfeld JV, Ford NL. Bomb blast, mild traumatic brain injury and psychiatric morbidity: a review. Injury. 2010; 41(5):437–443. [PubMed: 20189170]
8. Ruff R. Best practice guidelines for forensic neuropsychological examinations of patients with traumatic brain injury. J Head Trauma Rehabil. 2009; 24(2):131–140. [PubMed: 19333068]
9. Frederick RI, Bowden SC. Evaluating constructs represented by symptom validity tests in forensic neuropsychological assessment of traumatic brain injury. J Head Trauma Rehabil. 2009; 24(2):105–122. [PubMed: 19333066]
10. Bauer L, O'Bryant SE, Lynch JK, McCaffrey RJ, Fisher JM. Examining the Test Of Memory Malingering Trial 1 and Word Memory Test Immediate Recognition as screening tools for insufficient effort. Assessment. 2007; 14(3):215–222. [PubMed: 17690378]
11. Flaro L, Green P, Robertson E. Word Memory Test failure 23 times higher in mild brain injury than in parents seeking custody: the power of external incentives. Brain Inj. 2007; 21(4):373–383. [PubMed: 17487635]
12. Green P, Flaro L, Courtney J. Examining false positives on the Word Memory Test in adults with mild traumatic brain injury. Brain Inj. 2009; 23(9):741–750. [PubMed: 19636999]
13. Armistead-Jehle P. Symptom validity test performance in U.S. veterans referred for evaluation of mild TBI. Appl Neuropsychol. 2010; 17(1):52–59. [PubMed: 20146122]
14. Whitney KA, Shepard PH, Williams AL, Davis JJ, Adams KM. The Medical Symptom Validity Test in the evaluation of Operation Iraqi Freedom/Operation Enduring Freedom soldiers: a preliminary study. Arch Clin Neuropsychol. 2009; 24(2):145–152. [PubMed: 19395348]
15. Mac Donald CL, Johnson AM, Cooper D, Nelson EC, Werner NJ, Shimony JS, et al. Detection of blast-related traumatic brain injury in U.S. military personnel. N Engl J Med. 2011; 364(22):2091–2100. [PubMed: 21631321]
16. Matthews SC, Strigo IA, Simmons AN, O'Connell RM, Reinhardt LE, Moseley SA. A multimodal imaging study in U.S. veterans of Operations Iraqi and Enduring Freedom with and without major depression after blast-related concussion. Neuroimage. 2011; 54(Suppl 1):S69–S75. [PubMed: 20451622]
17. Peskind ER, Petrie EC, Cross DJ, Pagulayan K, McCraw K, Hoff D, et al. Cerebrocerebellar hypometabolism associated with repetitive blast exposure mild traumatic brain injury in 12 Iraq

war Veterans with persistent post-concussive symptoms. Neuroimage. 2011; 54(Suppl 1):S76–S82. [PubMed: 20385245]

18. Levin HS, Wilde E, Troyanskaya M, Petersen NJ, Scheibel R, Newsome M, et al. Diffusion tensor imaging of mild to moderate blast-related traumatic brain injury and its sequelae. J Neurotrauma. 2010; 27(4):683–694. [PubMed: 20088647]
19. Govindaraju V, Gauger GE, Manley GT, Ebel A, Meeker M, Maudsley AA. Volumetric proton spectroscopic imaging of mild traumatic brain injury. AJNR Am J Neuroradiol. 2004; 25(5):730–737. [PubMed: 15140711]
20. Babikian T, Freier MC, Ashwal S, Riggs ML, Burley T, Holshouser BA. MR spectroscopy: predicting long-term neuropsychological outcome following pediatric TBI. J Magn Reson Imaging. 2006; 24(4):801–811. [PubMed: 16941608]
21. Holshouser BA, Tong KA, Ashwal S, Oyoyo U, Ghamsary M, Saunders D, et al. Prospective longitudinal proton magnetic resonance spectroscopic imaging in adult traumatic brain injury. J Magn Reson Imaging. 2006; 24(1):33–40. [PubMed: 16755529]
22. Vagnozzi R, Signoretti S, Tavazzi B, Floris R, Ludovici A, Marziali S, et al. Temporal window of metabolic brain vulnerability to concussion: a pilot 1H-magnetic resonance spectroscopic study in concussed athletes--part III. Neurosurgery. 2008; 62(6):1286–1295. discussion 95-6. [PubMed: 18824995]
23. Henry LC, Tremblay S, Leclerc S, Khiat A, Boulanger Y, Ellemberg D, et al. Metabolic changes in concussed American football players during the acute and chronic post-injury phases. BMC Neurol. 2011; 11:105. [PubMed: 21861906]
24. Vaughan JT, Garwood M, Collins CM, Liu W, DelaBarre L, Adriany G, et al. 7T vs. 4T: RF power, homogeneity, and signal-to-noise comparison in head images. Magn Reson Med. 2001; 46(1):24–30. [PubMed: 11443707]
25. Avdievich NI, Hetherington HP, Kuznetsov AM, Pan JW. 7T head volume coils: improvements for rostral brain imaging. J Magn Reson Imaging. 2009; 29(2):461–465. [PubMed: 19161203]
26. Pan JW, Lo KM, Hetherington HP. Role of very high order and degree B0 shimming for spectroscopic imaging of the human brain at 7 tesla. Magn Reson Med. 2012; 68(4):1007–1017. [PubMed: 22213108]
27. Hetherington HP, Chu WJ, Gonen O, Pan JW. Robust fully automated shimming of the human brain for high-field 1H spectroscopic imaging. Magn Reson Med. 2006; 56(1):26–33. [PubMed: 16767750]
28. Avdievich NI, Pan JW, Baehring JM, Spencer DD, Hetherington HP. Short echo spectroscopic imaging of the human brain at 7T using transceiver arrays. Magn Reson Med. 2009; 62(1):17–25. [PubMed: 19365851]
29. Hetherington HP, Avdievich NI, Kuznetsov AM, Pan JW. RF shimming for spectroscopic localization in the human brain at 7T. Magn Reson Med. 2010; 63(1):9–19. [PubMed: 19918903]
30. Avdievich N. Transceiver-Phased Arrays for Human Brain Studies at 7T. Applied Magnetic Resonance. 2011; 41:483–506. [PubMed: 23516332]
31. Miyasaka N, Takahashi K, Hetherington HP. 1H NMR spectroscopic imaging of the mouse brain at 9.4T. J Magn Reson Imaging. 2006; 24(4):908–913. [PubMed: 16958063]
32. Hetherington HP, Kuzniecky RI, Vives K, Devinsky O, Pacia S, Luciano D, et al. A subcortical network of dysfunction in TLE measured by magnetic resonance spectroscopy. Neurology. 2007; 69(24):2256–2265. [PubMed: 18071146]
33. Cavus I, Pan JW, Hetherington HP, Abi-Saab W, Zaveri HP, Vives KP, et al. Decreased hippocampal volume on MRI is associated with increased extracellular glutamate in epilepsy patients. Epilepsia. 2008; 49(8):1358–1366. [PubMed: 18410365]
34. Benjamini Y, Hochberg Y. Controlling the false discovery rate: a practical and powerful approach to multiple testing. Journal of the Royal Statistical Society, Series B. 1995; 57(1):289–300.
35. Control. NCfIPa. Report to Congress on Mild Traumatic Brain Injury in the United States: Steps to Prevent a Serious Public Health Problem. Centers for Disease Control and Prevention. 2003
36. Stein MB, McAllister TW. Exploring the convergence of posttraumatic stress disorder and mild traumatic brain injury. Am J Psychiatry. 2009; 166(7):768–776. [PubMed: 19448186]

37. Hetherington HP, Pan JW, Mason GF, Adams D, Vaughn MJ, Twieg DB, et al. Quantitative 1H spectroscopic imaging of human brain at 4.1 T using image segmentation. Magn Reson Med. 1996; 36(1):21–29. [PubMed: 8795016]

38. Garman RH, Jenkins LW, Switzer RC 3rd, Bauman RA, Tong LC, Swauger PV, et al. Blast exposure in rats with body shielding is characterized primarily by diffuse axonal injury. J Neurotrauma. 2011; 28(6):947–959. [PubMed: 21449683]

39. Readnower RD, Chavko M, Adeeb S, Conroy MD, Pauly JR, McCarron RM, et al. Increase in blood-brain barrier permeability, oxidative stress, and activated microglia in a rat model of blast-induced traumatic brain injury. J Neurosci Res. 2010; 88(16):3530–3539. [PubMed: 20882564]

40. Svetlov SI, Prima V, Glushakova O, Svetlov A, Kirk DR, Gutierrez H, et al. Neuro-glial and systemic mechanisms of pathological responses in rat models of primary blast overpressure compared to "composite" blast. Front Neurol. 2012; 3:15. [PubMed: 22403567]

41. de Lanerolle NC, Bandak F, Kang D, Li AY, Du F, Swauger P, et al. Characteristics of an explosive blast-induced brain injury in an experimental model. J Neuropathol Exp Neurol. 2011; 70(11):1046–1057. [PubMed: 22002430]

42. Lu J, Ng KC, Ling G, Wu J, Poon DJ, Kan EM, et al. Effect of blast exposure on the brain structure and cognition in Macaca fascicularis. J Neurotrauma. 2012; 29(7):1434–1454. [PubMed: 21639720]

43. Hoge CW, McGurk D, Thomas JL, Cox AL, Engel CC, Castro CA. Mild traumatic brain injury in U.S. Soldiers returning from Iraq. N Engl J Med. 2008; 358(5):453–463. [PubMed: 18234750]

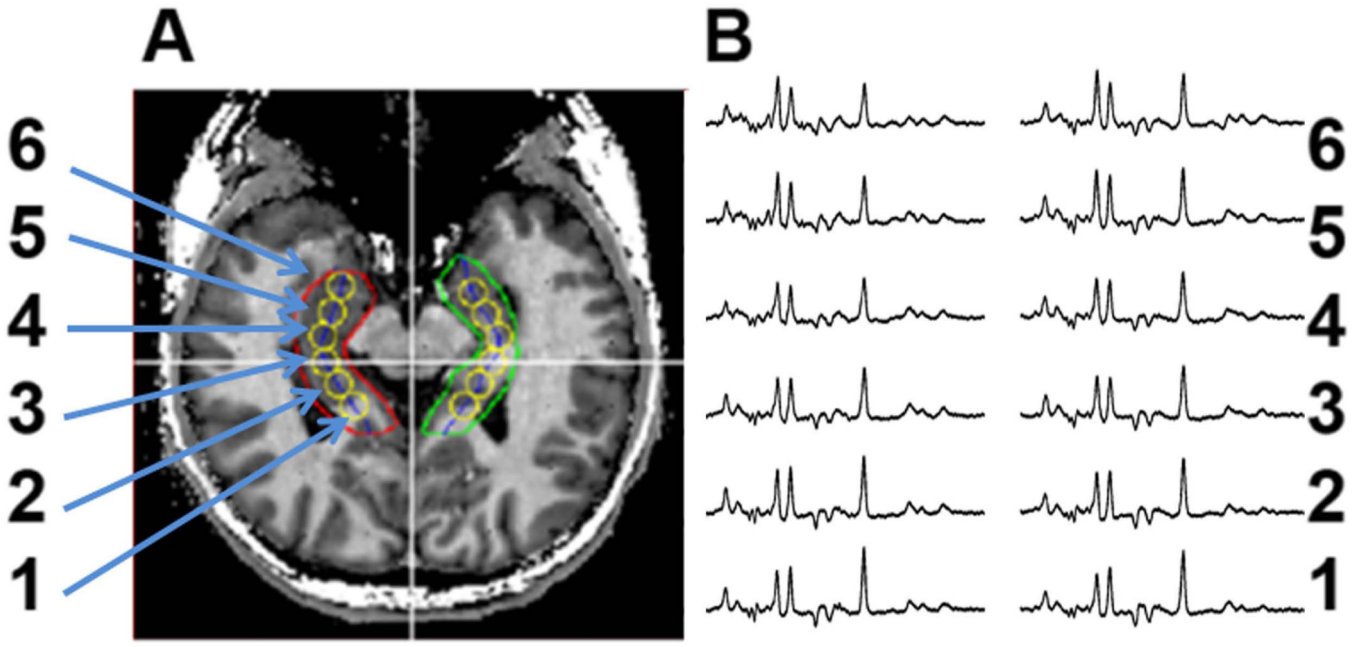

Figure 1.
Scout image showing the single voxel reconstruction (left) and spectra from the reconstructed loci (yellow circles) from a healthy control.

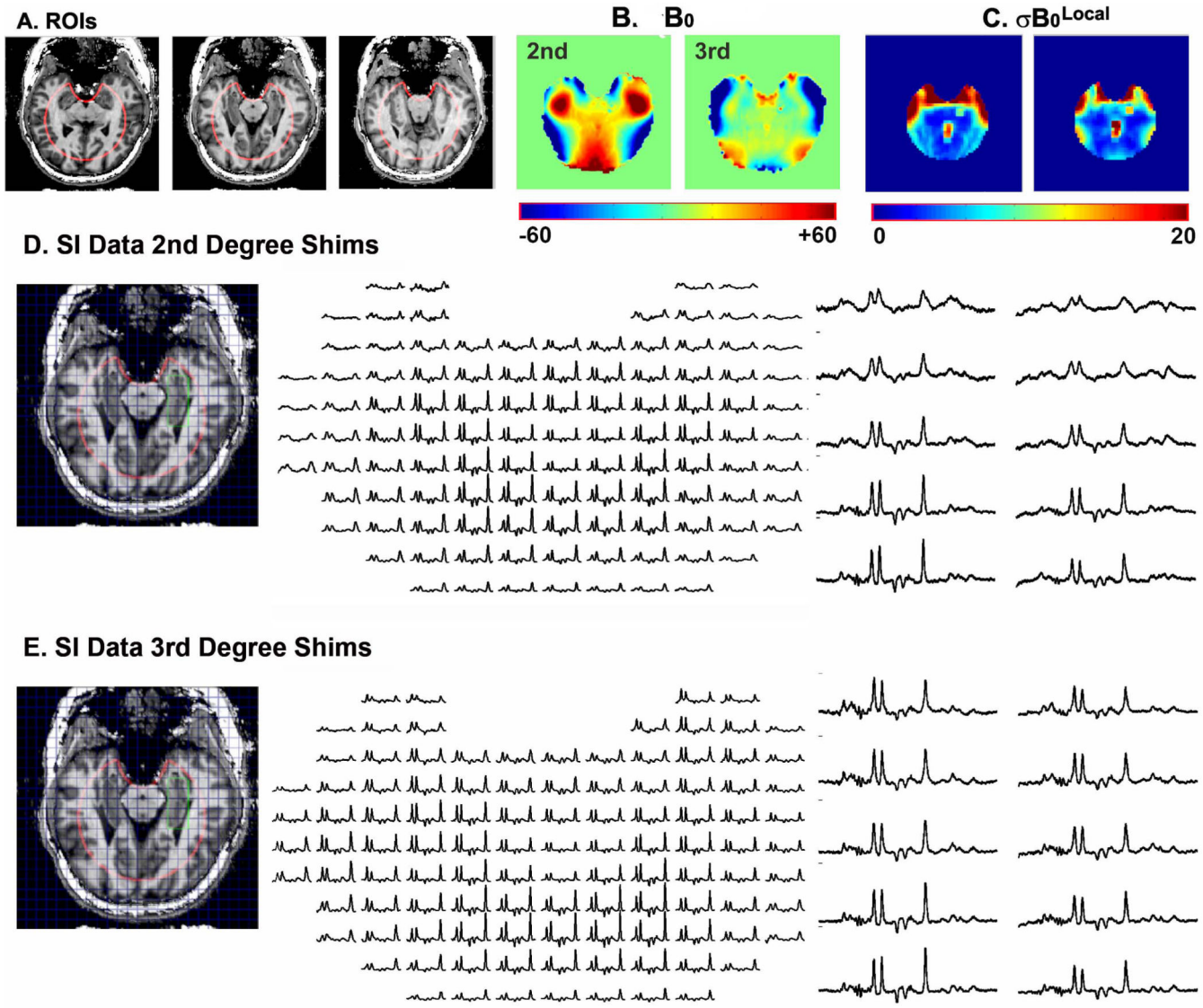

Figure 2.

2A- ROIs used for B_0 shimming; 2B - maps of B_0 using 1st&2nd degree (left) and 1st-3rd degree (right); 2C – maps of σB_0^{Local} using 1st&2nd degree (left) and 1st-3rd degree (right); 2D - MRSI data acquired with 1st&2nd degree shims (left) and single voxel reconstruction from the same data set (right); 2E - MRSI data acquired with 1st-3rd degree shims (left) and single voxel reconstruction from the same data set (right).

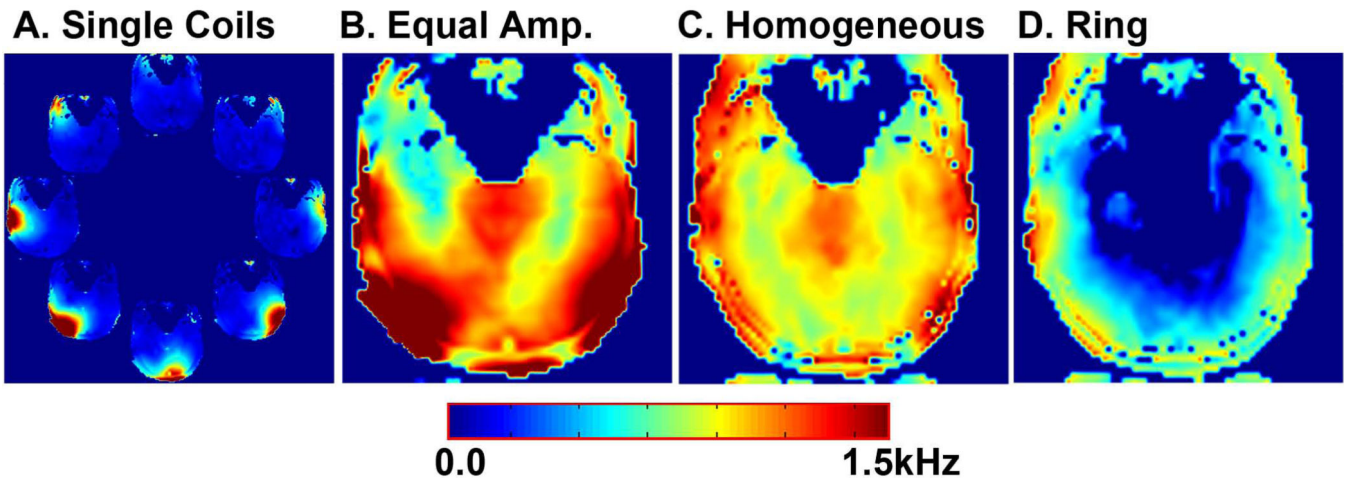

Figure 3.

3A – B_1^+ maps for individual coils; 3B – B_1^+ map for simultaneous transmission using equal amplitudes to all coils; 3C - B_1^+ map for the homogeneous distribution after B_1^+ shimming. 3D – B_1^+ map for the ring distribution.

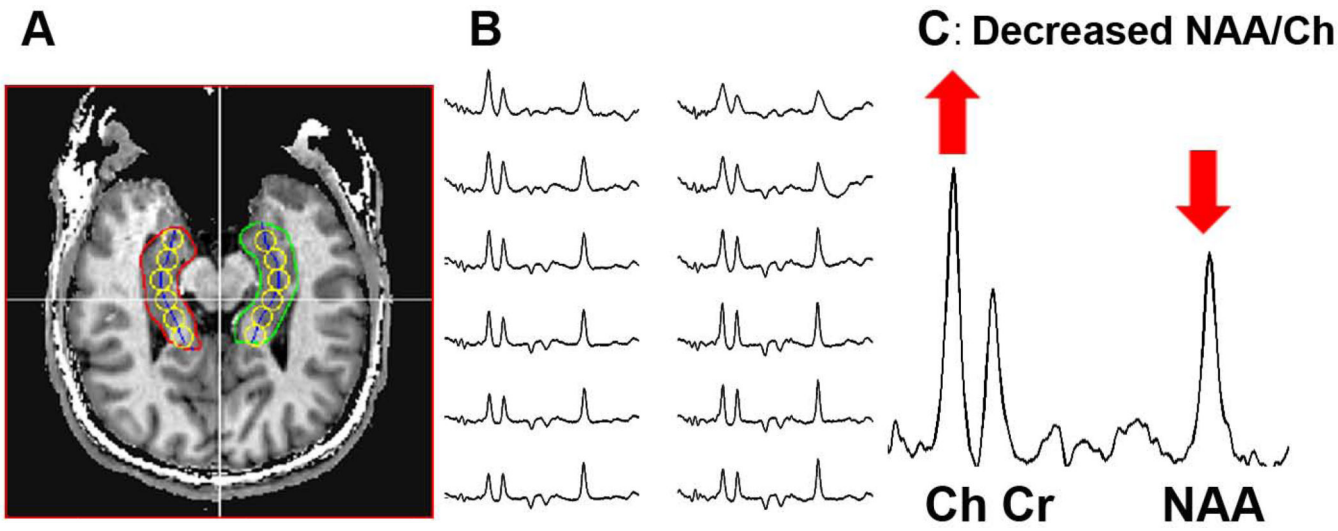

Figure 4.

Data from a veteran with blast mTBI. 4A - locations of the single voxel reconstructions (yellow circles); 4B spectra from these loci from a veteran with mTBI due to blast exposure; 4C - spectrum from the most anterior location of the right hippocampal formation.

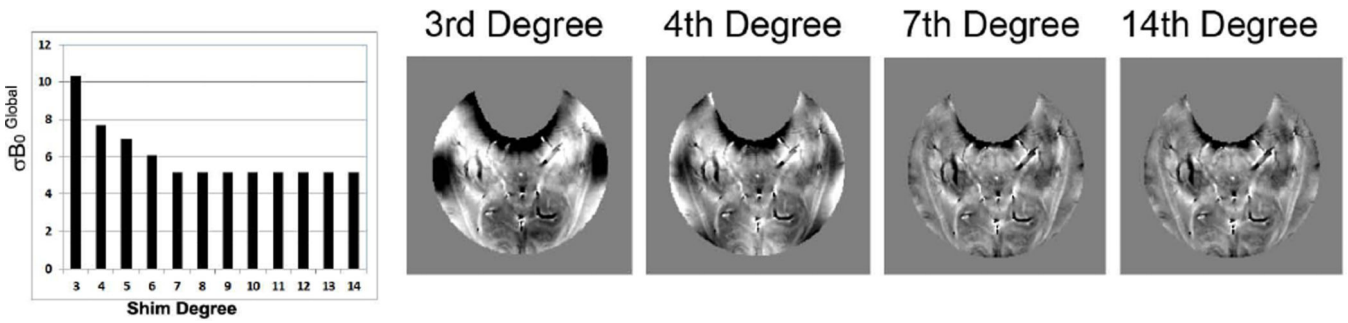

Figure 5.

σB_0^{Global} as a function of shim degree used and calculated B_0 maps using 3rd, 4th, 7th and 14th degree shims.

Table 1

σB_0^{Local} in Hz as a function of location along the hippocampal formation and ROI used for optimization.

σB_0^{Local}	**Tailored ROI**		**Whole Slice ROI**		**Tailored ROI: % improvement in σB_0^{Local}**
Location	**Mean Hz**	**SD Hz**	**Mean Hz**	**SD Hz**	**%**
1	3.83	2.58	4.42	2.65	13
2	3.81	1.71	4.13	2.01	8
3	4.62	3.30	6.03	3.64	23
4	7.34	4.32	8.49	4.59	14
5	9.37	5.77	11.18	5.99	16
6	11.43	5.89	14.61	6.95	22

Table 2

Average power (W) for individual coils in the array.

	Location	Homog. Avg. W	Homog. SD W	Ring Avg.W	Ring SD W	
23 cm	**Posterior**	147	50	18	6	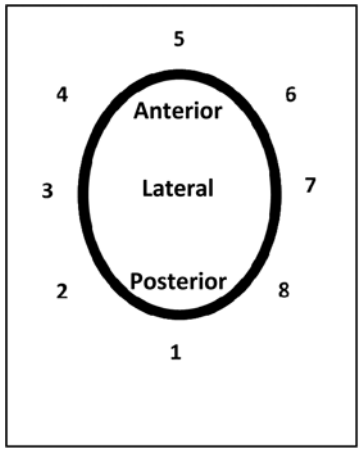
	Lateral	219	62	61	26	
	Anterior	432	116	131	14	
	Sum	2206	411	574	40	
25 cm	**Posterior**	181	74	24	12	
	Lateral	246	92	92	21	
	Anterior	539	111	131	12	
	Sum	2653	162	648	75	

Table 3

MRSI data for controls and patients.

				Left						Right					
NAA/Cr	**N**		**Age**	**1**	**2**	**3**	**4**	**5**	**6**	**1**	**2**	**3**	**4**	**5**	**6**
PATIENTS	25	**Avg**	34	1.50	1.31	1.29	1.27	1.15	1.18	1.46	1.30	*1.29*	**1.20**	*1.06*	**1.05**
		SD	9	0.17	0.11	0.16	0.20	0.15	0.19	0.16	0.08	*0.10*	**0.12**	*0.13*	**0.18**
		p value		NS	NS	NS	NS	NS	NS	NS	NS	*4.0E-02*	**3.5E-03**	*2.7E-02*	**5.6E-04**
CONTROL	20	**Avg**	32	1.47	1.32	1.33	1.32	1.21	1.21	1.46	1.34	1.37	1.31	1.17	1.29
		SD	12	0.15	0.10	0.12	0.17	0.17	0.17	0.16	0.10	0.12	0.11	0.16	0.22
NAA/Ch				**1**	**2**	**3**	**4**	**5**	**6**	**1**	**2**	**3**	**4**	**5**	**6**
PATIENTS	25	**Avg**	34	1.69	1.36	1.24	1.12	**0.95**	**0.86**	1.68	**1.37**	**1.26**	**1.11**	**0.92**	**0.81**
		SD	9	0.23	0.14	0.15	0.16	**0.15**	**0.18**	0.20	**0.14**	**0.16**	**0.17**	**0.14**	**0.19**
		p value		NS	NS	NS	NS	**1.04E-02**	**1.25E-02**	NS	**2.62E-02**	**1.03E-02**	**2.05E-02**	**3.72E-03**	**1.78E-05**
CONTROL	20	**Avg**	32	1.71	1.43	1.33	1.22	1.08	0.99	1.77	1.46	1.38	1.22	1.05	1.07
		SD	12	0.18	0.14	0.12	0.20	0.16	0.16	0.15	0.11	0.12	0.13	0.13	0.16

Bold p<0.05 and statistically significant after controlling for false discovery rate
Itallic p<0.05 but not statistically significant after controlling for false discovery rate.